A Long-Distance Underwater Wireless Optical Link Enabled by a Solar Array With a Baseline Compensator

Zhijian Tong, Xingqi Yang, Yunhai Gao, Hao Zhang, Yufan Zhang, Xiyin Wang, and Jing Xu

***Abstract*—In this paper, a self-designed solar cell-based optical detector is proposed and demonstrated in a long-distance underwater wireless optical communication (UWOC) link. Benefitting from a large detection area, the detector could successfully capture optical signals with a received power density of 5.62 $\mu W/cm^2$. To resist the baseline drift caused by the low-frequency cut-off of the system, an envelope detector-based baseline compensator is proposed. Comparing with digital solutions, the proposed compensator could be established in analog domain with common electronic components. With the compensator, a frequency domain equalizer (FDE) and a maximum ratio combing (MRC) algorithm, an 18 Mbps non-return-to-zero (NRZ) on-off keying (OOK) modulated link over an 80 m underwater channel is finally achieved. The proposed baseline compensator could compensate the low-frequency components effectively with low cost. Moreover, under a strong ambient light of approximately 1200 lux, the performance of the link shows little degradation. Our work shows a potential solution of long-distance UWOC system with ambient light tolerance, which is compatible with practical environment.**

***Index Terms*—Baseline drift, photoconductive, series-connection, solar array, underwater wireless optical communication.**

I. Introduction

With the ongoing activities of underwater exploration, huge amount of data are generated and a high-speed underwater communications system is in urgent need. Traditional solutions like underwater acoustic communications (UAC) suffer from low data rate and high latency [1], [2]. Underwater wireless optical communications (UWOC), featuring high speed and low latency, attracts attentions of lots of researchers [3], [4], [5]. A lot of progress has been made in recent years. In 2016, a compact and low power consumption UWOC system with a data rate of 1.5 Gbps over a 20-m underwater channel was demonstrated [6]. In the next year, a green laser-based UWOC system with a data rate of 2.70 Gbps over a 34.5-m underwater channel was demonstrated [7]. In 2019, a maximum data rate of 2.5 Gbps over a 60-m underwater channel was achieved with a non-return-to-zero (NRZ) on-off keying (OOK) modulated blue laser diode (LD) [8]. In the same year, with a high-power green laser diode, a 500-Mbps UWOC link supporting a 100-m underwater transmission was demonstrated using NRZ-OOK modulation [9]. With a discrete Fourier transform-spread (DFT-S) discrete multi-tone (DMT) modulation format, which is much more complex than commonly used baseband modulation schemes like OOK and pulse position modulation (PAM), a 5.6-Gbps UWOC link was achieved over an underwater transmission of 55-m [10]. With such a multi-carrier modulation and a pre-equalizer, the data rate of a light emitting diode (LED)-based UWOC system was improved to several Gbps as well [11]. In 2020, a 32-quadrature amplitude modulation (QAM) single-carrier UWOC system combining with frequency domain equalization and noise prediction (FDE-NP) was proposed as a promising alternative to multi-carrier schemes generally suffering from high peak to average power ratio (PAPR). And the proposed UWOC system, employing FDE-NP with a data rate of 3.31 Gbps, was demonstrated over a 56-m underwater channel [12]. Moreover, some researches show that the data rate of UWOC systems could reach up to tens of Gbps [13], [14], [15]. However, such high-speed UWOC systems usually require a precise link alignment, which hinders them from building and maintaining the optical link. The high requirement on link alignment is a huge barrier for applications in practical environments.

With the employment of high-sensitive detectors with relatively large active areas, like photomultiplier tubes (PMTs) and multi-pixel photon counters (MPPCs), the transmission distance was further extended while the optical system is simplified and the alignment requirement is relaxed. In 2017, a prototype with silicon photomultipliers (SiPMs) and LEDs was designed by IFERMER (French Research Institute for Exploitation of

Manuscript received 17 February 2023; revised 22 March 2023; accepted 1 April 2023. Date of publication 7 April 2023; date of current version 17 April 2023. This work was supported in part by the National Key Research and Development Program of China under Grants 2022YFC2808200 and 2022YFB2903403, in part by the National Natural Science Foundation of China (NSFC) under Grant 61971378, in part by the Strategic Priority Research Program of the Chinese Academy of Sciences under Grant XDA22030208, and in part by Zhoushan-Zhejiang University Joint Research Project under Grant 2019C81081. *(Corresponding author: Jing Xu.)*

Zhijian Tong, Xingqi Yang, Yunhai Gao, Hao Zhang, Yufan Zhang, and Xiyin Wang are with the Optical Communications Laboratory, Ocean College, Zhejiang University, Zhoushan 316021, China, and also with the ZTT-Ocean College Joint Research Center for Marine Optoelectronic Technology, Ocean College, Zhejiang University, Zhoushan 316021, China (e-mail: 11934055@zju.edu.cn; xq_y@zju.edu.cn; gaoyunhai@zju.edu.cn; hzhang20@zju.edu.cn; 12034050@zju.edu.cn; 22134017@zju.edu.cn).

Jing Xu is with the Optical Communications Laboratory, Ocean College, Zhejiang University, Zhoushan 316021, China, also with the Hainan Institute of Zhejiang University, Sanya, Hainan 572025, China, and also with the ZTT-Ocean College Joint Research Center for Marine Optoelectronic Technology, Ocean College, Zhejiang University, Zhoushan 316021, China (e-mail: jxu-optics@zju.edu.cn).

Digital Object Identifier 10.1109/JPHOT.2023.3264445

the Sea), which achieved a data rate of 3 Mbps over a 60-m underwater channel with an attenuation length (AL) of 9. The active area of the arrayed SiPM-based detector is 36 mm^2 and the field of view (FOV) is wider than 30° [16]. In 2020, a UWOC system that could work within weak turbulence over 10 AL was proposed, achieving a data rate of 1 Gbps with an SiPM [17]. With an optical combination of three high-power fiber-pigtailed LDs and arrayed MPPCs, a 100-m underwater link was demonstrated with a maximum data rate of 8.39 Mbps while the alignment requirement was relaxed [18]. Based on high-sensitive detectors and modern digital signal processing (DSP) schemes, the performance of the long-distance UWOC system was further improved. In 2021, with a variable step size generalized orthogonal matching pursuit, a 500-Mbps underwater link was achieved over a 200-m underwater channel [19]. This year, a 3-Gbps/100-m underwater link was reported, which was the first Gbps-class UWOC experimental demonstration with a transmission distance of 100 m that had ever been reported [20].

However, most of the researches aim at extending the transmission distances and improving the data rates, ignoring the impact of environmental illuminations. Though the deployment of high-sensitive detectors makes it easy to build long-distance UWOC links, the characteristics of such detectors determine that background light will influence the system performance severely, which might limit the practical application of UWOC systems. For example, such a UWOC system usually cannot work properly in shallow water. It has been proved that a solar cell-based detector could work under ambient light with simultaneous energy harvesting [24], [25], [26], [27], [28], indicating that solar cell-based detectors could work under ambient lights. Moreover, with the advantage of large detection area, a solar array can effectively relax the requirement of link alignment. It has been proved that cost-effective solar cell-based receivers have great potentials in UWOC applications. In 2014, a solar panel was adopted as an optical detector of an optical wireless communication (OWC) system, achieving a data rate of 1 Mbps with an OOK modulated signal and 7.01 Mbps with an OFDM modulated signal, respectively [21]. The work shows the feasibility of using solar panels as detectors of optical communication links. In 2018, we investigated the superiority of a solar panel used as a lens-free detector in a UWOC system and built an OFDM modulated underwater link with a maximum data rate of 22.56 Mbps with an underwater transmission of 7 m [22]. Solar cell-based detectors could effectively relax the alignment requirement between the transmitter and the receiver, benefitting from its large detection area. In the next year, with diversity reception and maximum ratio combining (MRC), the data rate of the proposed solar cell-based UWOC system was improved to 84 Mbps with 16-QAM-OFDM signals [23]. Besides, the applications of simultaneously detecting optical signals and harvesting energy are investigated. In 2020, a 784-Mbps optical link with a tiny photovoltaic (PV) GaAs cell was achieved with the energy harvesting efficiency of 41.7% at the expense of losing the superiority of large detection area [24]. A reverse bias could effectively widen the depletion area of a PN junction, thus improving its responsivity and frequency response. With the adoption of a reverse bias, a data rate of 17.05 Mbps was achieved with a DMT scheme while the solar energy conversion efficiency was also enhanced [25]. Moreover, it has been proved that organic solar cells are also suitable for such applications. Combining with an OFDM-modulated signal, a data rate of 34.2 Mbps was achieved with a solar cell-based UWOC system while harvesting an electrical power of 0.43 mW [26]. Taking the advantage of the high light absorption coefficient of amorphous silicon thin-film solar cells, an energy-autonomous optical communication prototype named AquaE-lite was developed, achieving a data rate of 1.2 Mbps over a 2-m underwater channel [27], [28]. In 2021, we connected several solar cells in series and applied a reverse bias on the solar array to improve the frequency response. The −20-dB bandwidth of the 3 × 3 solar array was extended to 63.4 MHz, and a maximum data rate of 150 Mbps over a 35-m underwater channel was achieved [29].

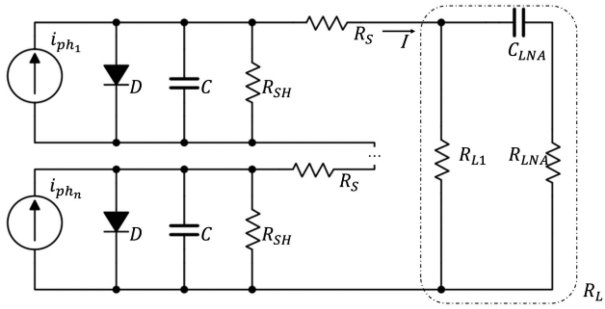

Fig. 1. Equivalent circuit of the series-connected solar array.

In this work, we investigate the performance of a reverse-biased solar array under weak optical signals and strong environmental illuminations. Featuring large detection area, four solar arrays are adopted as the detector in a long-distance UWOC system. To deal with the baseline drift caused by the bandpass transmission, an envelope detector-based compensator is proposed. Four solar arrays with large detection area are adopted for diversity reception to improve the signal to noise ratio (SNR) of the received signal. Combining with the proposed baseline compensator and an FDE, a maximum data rate of 18 Mbps is achieved over an 80-m underwater channel under common indoor lighting environment with NRZ-OOK modulation. Ambient light is a significant factor that influences the performance of a sensitive detector-based long-distance UWOC system. Our work shows that the ambient light has little effect on the performance of the proposed solar array-based UWOC system, which could facilitate its application in shallow water. We figure that it is a potential cost-effective solution to the practical application of long-distance UWOC systems with strong ambient light tolerance.

II. Principles and Simulations

A. A Solar Array-Based Detector

In [29], we have investigated the performance of the solar array under relatively high optical power density, showing that solar arrays have great potentials in detecting high-speed optical signals. Considering the input impedance of the low noise amplifier (LNA), the equivalent circuit of the proposed solar array-based detector is shown in Fig. 1.

Based on the equations of the frequency response of the solar array we have given in [29], combining with the input impedance of the LNA, the frequency of the solar array-based detector can be expressed as:

$$\left|\frac{v(\omega)}{I_{PH}(\omega)}\right|^2 = \left|\frac{\frac{R_L}{R_L+nR_s+\frac{(n-1)R_{SH}}{j\omega CR_{SH}+1}}}{\frac{1}{r}+\frac{1}{1/j\omega C}+\frac{1}{R_{SH}}+\frac{1}{R_L+nR_s+\frac{(n-1)R_{SH}}{j\omega CR_{SH}+1}}} \times \frac{R_{LNA}}{\frac{1}{j\omega C_{LNA}}+R_{LNA}}\right|^2, \quad (1)$$

where ω is the angular frequency and r is the small-signal equivalent resistor of the diode D. $I_{PH}(\omega) = \sum_1^n i_{PH}(\omega)$is the AC component of the photocurrent generated by the solar array, which is proportional to the optical power captured by the array. R_{LNA} is the input impedance of the LNA and C_{LNA} is the capacitance of the DC-blocking capacitor in the LNA. R_L is the equivalent load resistance of the peripheral circuit directly connected to the solar array shown in the dashed box in Fig. 1, which is:

$$R_L = \frac{R_{L1}\left(j\omega C_{LNA}R_{LNA}+1\right)}{1+j\omega C_{LNA}\left(R_{L1}+R_{LNA}\right)}. \quad (2)$$

From the equations we have given in [29] and the frequency response shown by (1), we can get the conclusion that the frequency response of the detector is mainly determined by the number of cells in the array and the load resistance R_{L1}. It is worth noticing that the equivalent resistor r is considered to be stable when dealing with small signals. Actually, it is related to the voltage across the diode. The current through the parasitic diode I_D can be calculated by the Shockley equation, which is:

$$I_D = I_0\left(e^{\frac{V_D}{nV_{TH}}}-1\right), \quad (3)$$

where I_0 is the reverse saturation current of the diode, and $V_{TH} = k_BT/q$ is the thermal voltage. According to (1) and (3), a small V_D, which is positively associated with the load resistor R_L, helps to mitigate the nonlinearity of the output.

To better investigate the influences of the factors, the model is simulated with the parameters given in [30], which is shown in Table I.

From the simulated results shown in Fig. 2, we can get the conclusion that connecting solar cells in series is an effective way to improve the frequency response, which is the main restriction of the solar cell-based UWOC system. However, as shown in Fig. 2(b), the bandwidth increasement mitigates as the number of the cells increases. Moreover, when the number of the cells increases, to guarantee the average voltage of the reverse bias on each cell, a higher voltage of the reverse bias applied on the array is required. In conclusion, considering the trade-off between the bandwidth increasement and the high voltage required by the module, we figure that approximately 10 cells would be an appropriate choice.

The simulated frequency response of the proposed detector with different values of the load resistor R_{L1} is shown in

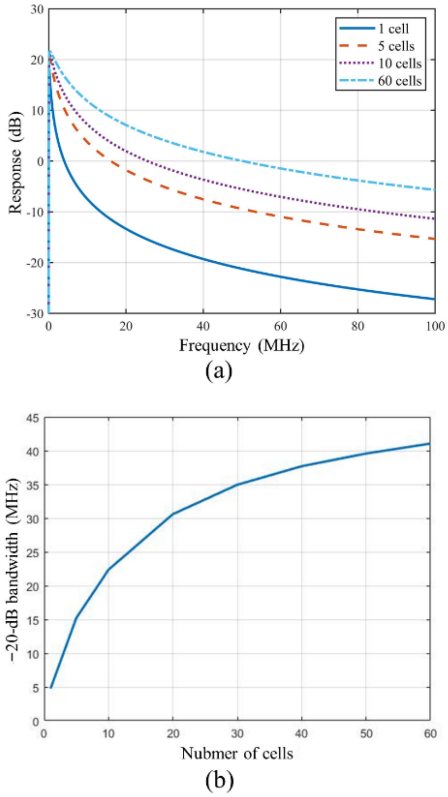

Fig. 2. (a) The simulated frequency response for different cell numbers, (b) the simulated −20-dB bandwidth for different cell numbers ($R_{L1} = 20\,\Omega$).

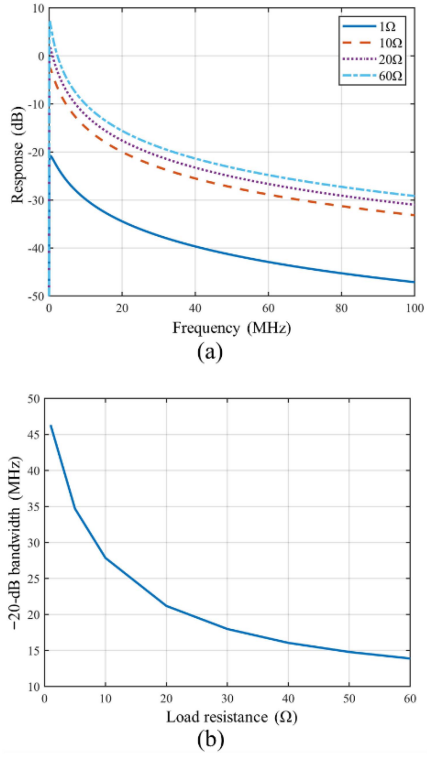

Fig. 3. The simulated frequency response with different load resistors, (b) the simulated −20-dB bandwidth with different load resistors (n = 9).

TABLE I
THE PARAMETERS USED IN THE SIMULATIONS

Parameter	Value
Series resistance R_S	1 Ω
Shunt resistance R_{SH}	20 kΩ
Junction capacitance C	34 nF
DC-blocking capacitance C_1	100 nF
Load resistance R_{L1}	1~60 Ω
Impedance of the LNA R_{LNA}	50 Ω
Equivalent resistance of the diode r	720 Ω
Number of the cells in the array n	1~60

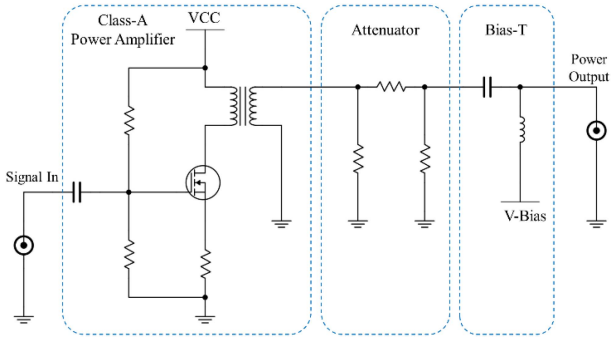

Fig. 4. Simplified diagram of the commonly used driver of the light source.

Fig. 3(a). Because of the low-pass filter formed by the junction capacitance and the load resistor, a smaller load resistor contributes to a higher bandwidth. On the other hand, according to Ohm's law, a smaller load resistor results in a smaller amplitude. Therefore, there is a trade-off between the bandwidth and the amplitude of the output signals.

B. The Baseline Drift of the Signal and the Solutions

In most of the reported UWOC systems, the electrical signal usually passes through a power amplifier (PA), an electrical attenuator and a bias-T to drive the light source, as shown in Fig. 4.

In this scheme, the power amplifier is used to enhance the power of the signal so that the LD could be driven effectively. Considering that the light source can only send a unipolar positive signal, a bias-T is used to superpose the signal and a DC voltage, so that the waveform could be completely covered by the linear region of the light source. However, the output impedance of the power amplifier commonly used is typically designed as 50 Ω, which is much larger than the equivalent impedance of the high-power LD in linear region. Take a commonly-used LD NICHIA NDB7875 as an example, the V-I curve of which is shown in Fig. 5. The slope of linear region of the curve is approximately 2 Ω, which is much smaller than the output impedance of the power amplifier. If the LD is connected to a PA directly, the mismatch of the impedance will cause severe reflections of the signal, leading to a distortion of the signal. Moreover, the reflected power may damage the output stage

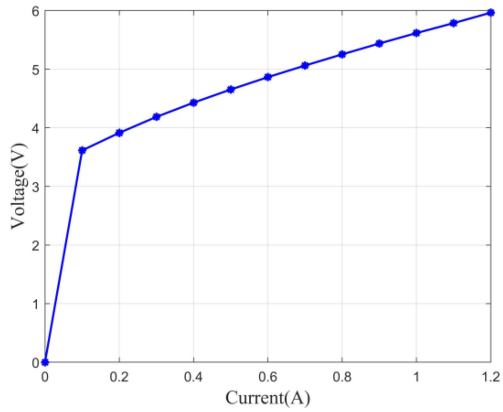

Fig. 5. The V-I curve of the LD NDB7875.

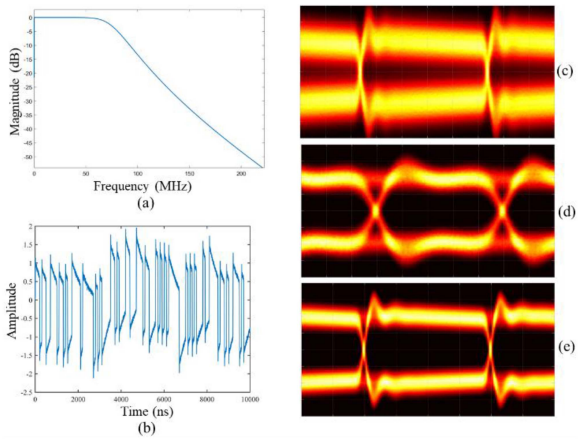

Fig. 6. (a) The frequency response of the bandpass system for simulation, (b) the waveform of the 10-Mbps NRZ-OOK signal passed through the bandpass system, (c) the eye diagram of the 10-Mbps NRZ-OOK waveform, (d) the eye diagram of the 40-Mbps NRZ-OOK waveform, (e) the eye diagram of the 10-Mbps 4B/5B-NRZI coded waveform.

of the PA permanently. According to [31], an attenuator could effectively reduce the voltage standing wave ratio (VSWR) in the line, so the attenuator is necessary to alleviate the distortion of the signal despite that it would decrease the electric power input to the LD.

As shown in Fig. 4, the input and output of the driver is AC coupled so the low frequency component of the signal cannot pass through. The low-frequency cutoff may cause the drift of the baseline of the signal [32], which has adverse effects on the system performance especially when the data rate is not high enough. To make the phenomenon clearly, a 10-stage Butterworth bandpass filter is used for simulation. The normalized frequency response of the filter is shown in Fig. 6(a), with a −3-dB passband from 100 kHz to 75MHz. As the simulated results shown in Fig. 6(b)–(d), when a 10-Mbps NRZ-OOK modulated signal passes through the bandpass system, a severe baseline drift is occurred, leading to a poor eye diagram. For comparison, when the data rate of the signal reaches up to 40 Mbps, the influence of the low-frequency cutoff is almost negligible thanks to the short symbol period.

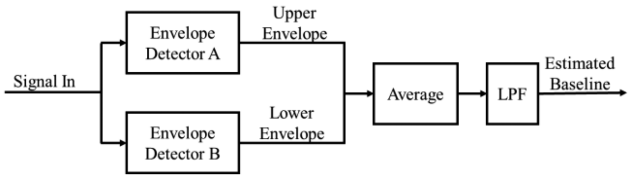

Fig. 7. The structure of the envelope detector-based compensator.

Therefore, the baseline drift of the signal is a key factor that influences the performance when the data rate is not high enough, especially when the SNR of the received signal is relatively low. Usually, length-limited coding is an effective solution to resist the low-frequency cutoff, which could reduce the low-frequency component of the spectrum, making it consistent with the bandpass transmission characteristic of the system. For example, 4B/5B-NRZI coding, which is widely used in Fiber Distributed Data Interface (FDDI) network, ensures a maximum number of continuous symbols less than 5. The eye diagram of the 10-Mbps 4B/5B-NRZI coded waveform is shown in Fig. 6(e), which illustrates that such coding schemes could effectively resist baseline drift. However, such coding scheme usually comes at the cost of additional bits [33]. 4B/5B-NRZI coding adds 1 bit for every 4 bits, resulting in a code efficiency of 80%.

In addition, a baseline drift compensator is an alternative solution to mitigate the impairment caused by the baseline drift without sacrificing the spectrum efficiency. A median filter or a wavelet transform scheme is commonly adopted to compensate for the drift in the receiver. However, such scheme can only be implemented in the digital domain, causing an extra computational cost. In some low power embedded applications, the computing power required by DSP may not be satisfied, an analog solution is an alternative. In this work, an envelope detector-based compensator is adopted to compensate for the drift when dealing with the captured signal. The structure of the compensator is shown in Fig. 7, two envelope detectors are adopted to detect the upper envelope and the lower envelope. Then a pre-estimated baseline curve is obtained by calculating the average values of the acquired envelopes. A low pass filter (LPF) is adopted to remove the high-frequency fluctuations of the curve and finally get the estimated baseline.

Comparing with the digital solutions, the proposed envelope detector-based solution can be easily realized with common electronic components like capacitors and resistors, as shown in Fig. 8(a). The assembled printed circuit board (PCB) is shown in Fig. 8(b). With the waveform in Fig. 6(b) passing through the module, the waveforms of the estimated baseline and the signal are shown in Fig. 9(a). Comparing the eye diagrams before and after compensation, which are shown in Figs. 6(c) and 9(b) respectively, the eye height of the diagram is significantly improved. The frequency spectrum of the signals before and after compensation are shown in Fig. 9(c) and (d). The low-frequency component of the signal is effectively compensated, resulting in an improved performance.

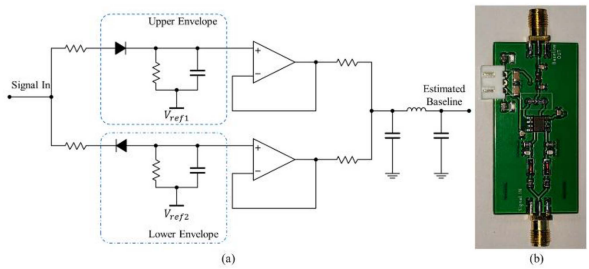

Fig. 8. (a) A simplified example of the envelope detector-based baseline estimator, (b) the assembled PCB of the estimator.

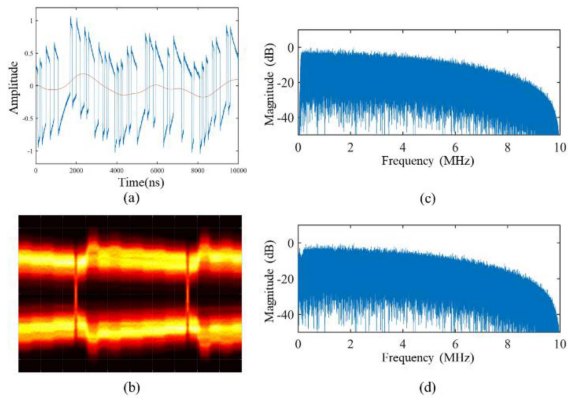

Fig. 9. (a) The waveform of the signal and the estimated baseline, (b) the eye diagram of the compensated waveform, (c) the frequency spectrum of the waveform before compensation, (d) the frequency spectrum of the compensated waveform.

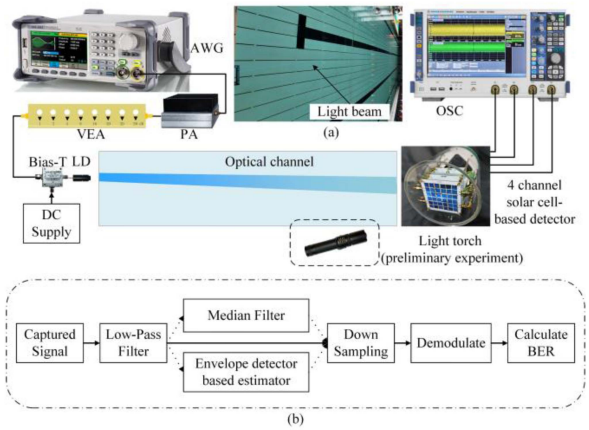

Fig. 10. Experimental setup of the proposed UWOC system, (a) the underwater channel in the swimming pool, (b) the diagram of the digital signal processing in the receiver.

III. Experimental Setup

The experiments were conducted both in our laboratory and a swimming pool and the experimental setup is shown in Fig. 10. At the transmitter side, an offline generated OOK-modulated signal was fed into an arbitrary wave generator (AWG, SDG6012X-E). Then the power of the output signal was amplified by a PA (37 dB, 100 kHz∼75 MHz). Considering the impedance of the LD (NICHIA NDB7875), a key-press variable electrical attenuator (VEA, KT3.0-90/1S-2S) was connected right behind

the PA to balance the input impedance of the LD and the output impedance of the PA as well as adjust the amplitude of the signal. After combining the bipolar signal and the bias voltage with a bias-T (Mini-Circuits ZFBT-4R2GW), the signal was finally fed into the blue-light LD and converted into an optical signal. At the receiver side, a self-designed four-channel solar cell-based detector fixed in a watertight cabin, was used to capture the optical signal. The detector consists of 36 solar cells, the size of which is 1 cm $\times$ 1 cm, resulting in a total active area of 36 cm^2. To simplify the circuit of the proposed detector, the revere bias of the four solar arrays in the detector shared a step-up DC to DC converter. Finally, the signals recorded by four channels of an oscilloscope (OSC, Rohde & Schwarz RTO2024) were processed offline on a computer. The diagram of the digital signal processing on the computer is shown in Fig. 10(b).

A preliminary laboratory experiment was conducted first, to optimize the parameters of the experiment to be conducted in the pool as well as verify the simulation results. During the experiment, the driving current of the DC bias is set to 0.45 A and the amplitude of the signal output from the AWG is 500 mV. The optical power generated by the LD is approximately 26.5 dBm. In the laboratory, the optical channel is in the air and a variable neutral density (ND) filter was set in front of the LD to adjust the optical power on the detection plane. To investigate the performance of the proposed detector under ambient lights, a light torch, as shown in the dashed box in Fig. 10, was put in front of the detector to generate a strong background light. In the swimming pool experiment, the optical channel refers to an 80-m underwater channel in a standard swimming pool with a mirror to reflect the light beam. The experiment was conducted under common indoor illuminations, as shown in Fig. 10(a).

IV. Results and Discussions

We have investigated the performance with different cell numbers in the array under different reverse bias voltages in [29]. The consistency between the reported experimental results and the simulation results in Section II verifies the correctness of the model. The conclusion we have drawn is that connecting solar cells in series and applying a reverse bias on the array are effective ways to improve the frequency response. In this experiment, a reverse bias is also applied to the arrays installed in the detector cabin.

In the preliminary experiment, the performance of the proposed system with different load resistances R_L was investigated and the result is shown in Fig. 11. Because the four arrays share the same DC supply, crosstalk between four channels causes a little degradation of the frequency response. As the load resistance increases from 10 Ω to 60 Ω, the −20-dB bandwidth of the system decreases from 58 MHz to 39 MHz. When the load resistance decreases, the amplitude of the signal output by the LNA is decreased as well. Because of the imperfect electromagnetic shielding as well as the parasitic parameters, the curves in Fig. 11 fluctuate and cross with each other, and they are not as smooth as the simulated curves shown in Fig. 3(a). However, the trend of the curves is consistent with the simulation results, showing that the system bandwidth is negatively correlated with the load resistance. Because of the extra noises introduced by the LNAs connected to the array, the SNR will decrease sharply if the input signal is too weak. It can be concluded that the system bandwidth is negatively correlated with the load resistance, which is consistent with the simulation results. Considering the trade-off between the bandwidth and the amplitude of the signal, we figure that 20 Ω is a proper load resistance, maintaining an ideal frequency response and a relatively high amplitude.

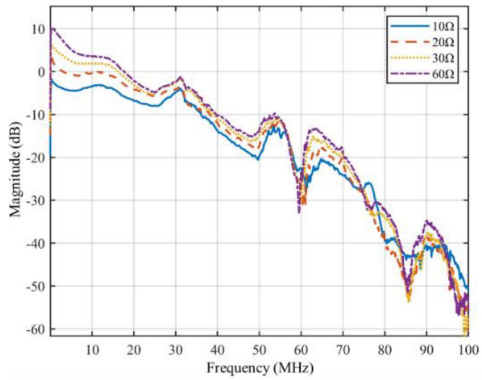

Fig. 11. The frequency response of the proposed system with different load resistances.

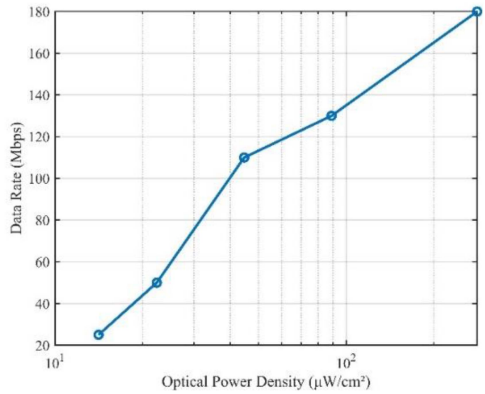

Fig. 12. The maximum achievable data rate under different optical power densities.

In the following communication experiment, the load resistance was set to 20 Ω and the size of the solar array was set to 3 $\times$ 3. Then the performance difference of the system under different signal powers is investigated in the preliminary experiment. A solar cell-based detector consisting of 4 sets of 3 $\times$ 3 array is adopted in the experimental system with an active area of 36 cm^2. The optical power on the detection plane is measured by an optical power meter (Thorlabs PM100D) with a power sensor of S130C. As mentioned in the specifications sheet of the sensor, the diameter of the input window is 9.5 mm. A power density is used for illustration as the active areas of the proposed detector and the sensor of the power meter are quite different. The maximum achievable data rate under different optical power densities are shown in Fig. 12. As the optical power density on the detection plane increases from 14.12 $\mu W/cm^2$ to 281.63 $\mu W/cm^2$, the achievable maximum data rate increases from 25 Mbps to 180 Mbps. When the optical power density

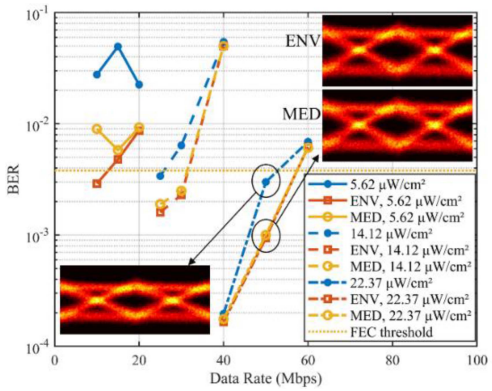

Fig. 13. Comparisons between the BERs when using different compensators. Insets: The eye diagrams with or without a compensator. (ENV: Compensate with an envelope detector-based compensator, MED: Compensate with a median filter-based compensator).

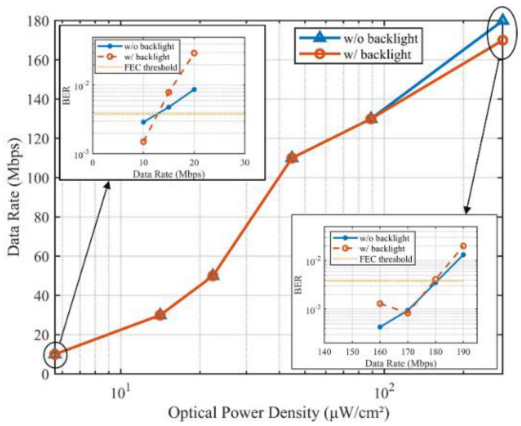

Fig. 14. The maximum data rate under different signal powers with or without background light with the proposed envelope detector-based compensators. Insets: the BER versus data rate of the testing points.

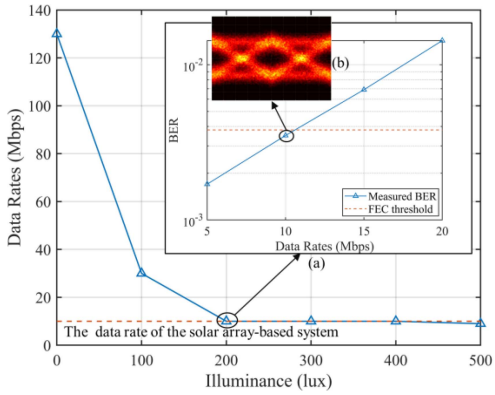

Fig. 15. The maximum data rate of the MPPC-based system under different ambient illuminations. (a) the BER versus data rate of the testing point, (b) the eye diagrams of the testing point.

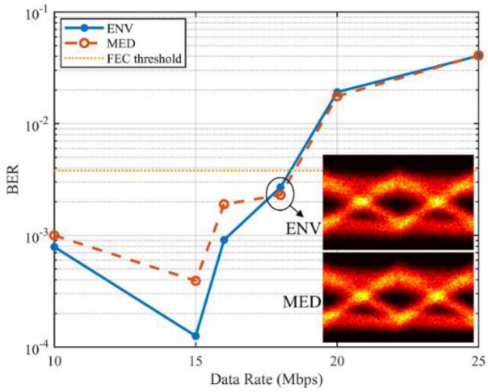

Fig. 16. Measured BER verses data rate over an 80-m underwater channel. Insets: the eye diagrams of the signal with different compensators.

is as low as 5.62 $\mu\mathrm{W/cm^2}$, the average bit error rate (BER) of a 10-Mbps link is 1.56×10^{-2}, which is higher than the FEC threshold. According to the phenomenon observed in the experiment, the SNR decreases sharply when the power density of the optical signal is lower than 44.64 $\mu\mathrm{W/cm^2}$, leading to the rapidly deteriorating of the performance. When the optical power is lower than 14.12 $\mu\mathrm{W/cm^2}$, it is hard to build an efficient optical link because of the poor SNR and the errors caused by the baseline drift. To reduce the BER to a certain extent, a proposed envelope detector-based compensator is adopted to compensate for the drift, As shown in Fig. 13 . When the data rate is lower than 40 Mbps under an optical power density of 5.62 $\mu\mathrm{W/cm^2}$, the BER performance of the system is affected by both the frequency response of the system and the drift of the baseline. As the data rate decreases, the drift of the baseline becomes apparent while the influence of bandwidth is weakened. At such circumstances, the proposed drift compensator reduces the BER effectively, and the BER of the 10-Mbps transmission under an optical power density of 5.62 $\mu\mathrm{W/cm^2}$ reduces from 1.56×10^{-2} to 2.9×10^{-3}. Besides, a median filter-based compensator is adopted for comparison, the proposed compensator works a little better than a median filter-based compensator in most instances.

Ambient light is a key factor that influences the performance of high-sensitive detector-based UWOC systems, which limits the applications in shallow water. The performance of the proposed system is investigated under a strong background light generated by a torch. The illuminance measured on the detecting plane is approximately 1200 lux. The little difference between two curves in Fig. 14 proves that background light has little effect on the system performance as long as the solar array is not saturated.

Although an MPPC is highly sensitive, it generally cannot work properly with ambient illuminations. For comparison, an MPPC is adopted as the receiver in the proposed UWOC system. The maximum data rates of the MPPC-based system with the optical power density of 5.62 $\mu\mathrm{W/cm^2}$ under different ambient illuminations are shown in Fig. 15. Thanks to high sensitivity of the MPPC, when the environment is dark enough, the maximum data rate reaches up to 130 Mbps, which is much higher than that of the solar array-based system. But when the illuminance increases, the performance of the MPPC decreases sharply. When the illuminance is higher than 200 lux, the performance of the MPPC-based system is almost the same as that of the proposed solar-array based system. Thus, a solar array can be considered as an interesting low-cost alternative for long-distance UWOC under ambient illuminations.

To further demonstrate the performance of the proposed solar array-based UWOC system, an experiment was conducted in a standard swimming pool under common indoor illumination. The attenuation coefficient of the water in the swimming pool is measured to be about 0.33 dB/m. After transmitting over an 80-m underwater channel, the power density of the optical signal measured on the receiving plane is about 13.47 $\mu\mathrm{W}/\mathrm{cm}^2$. The BER performance of the system with different data rates is shown in Fig. 16.

With the drift compensator, the optical link was built successfully over an 80-m underwater channel in the swimming pool. The maximum achieved data rate is 18 Mbps with the BER lower than the FEC threshold of 3.8×10^{-3}. The performance measured in the swimming pool agrees with the results of the preliminary experiment.

V. Conclusion

In this work, a self-designed solar cell-based detector was adopted in a long-distance UWOC link. To further increase the detection area, four 3×3 solar arrays were integrated in a watertight cabin, resulting in an active area of 36 cm^2. In the preliminary experiment, the performance of the proposed system is investigated with or without ambient lights. Under a strong illuminance generated by a light torch, there is little degradation on the performance of the proposed solar cell-based detector, enabling ideal performances in different light environments. With the proposed envelope detector-based drift compensator, an MRC algorithm and an FDE, an 18-Mbps underwater link was successfully achieved over an 80-m underwater channel under common indoor illuminations. It has been proven that the proposed system works properly in the environment with ambient light, which is close to practical environment. Our work shows the potential of a solar array-based detector for long-distance UWOC applications with strong ambient light tolerance.

References

[1] M. F. Ali, D. Jayakody, Y. Chursin, S. Affes, and S. Dmitry, "Recent advances and future directions on underwater wireless communications," *Arch. Comput. Methods Eng.*, vol. 26, no. 100, pp. 1–34, 2019.

[2] J. H. Goh, A. Shaw, and A. I. Al-Shamma'a, "Underwater wireless communication system," *J. Phys. Conf.*, vol. 178, 2009, Art. no. 012029.

[3] H. Kaushal and G. Kaddoum, "Underwater optical wireless communication," *IEEE Access,* vol. 4, pp. 1518–1547, 2016.

[4] Z. Zeng, S. Fu, H. Zhang, Y. Dong, and J. Cheng, "A survey of underwater optical wireless communications," *IEEE Commun. Surv. Tut.*, vol. 19, no. 1, pp. 204–238, Firstquarter 2017.

[5] J. Xu, "Underwater wireless optical communication: Why, what, and how? [Invited]," *Chin. Opt. Lett.*, vol. 17, no. 10, pp. 38–47, 2019.

[6] C. Shen et al., "20-meter underwater wireless optical communication link with 1.5 Gbps data rate," *Opt. Exp.*, vol. 24, pp. 25502–25509, 2016.

[7] X. Liu et al., "34.5 m underwater optical wireless communication with 2.70 Gbps data rate based on a green laser diode with NRZ-OOK modulation," *Opt. Exp.*, vol. 25, no. 22, pp. 27937–27947, 2017.

[8] C. Lu, J. Wang, S. Li, and Z. Xu, "60 m/2.5 Gbps Underwater optical wireless communication with NRZ-OOK modulation and digital nonlinear equalization," in *Proc. Conf. Lasers Electro-Opt.*, 2019, pp. 1–2.

[9] J. Wang, C. Lu, S. Li, and Z. Xu, "100 m/500 Mbps underwater optical wireless communication using an NRZ-OOK modulated 520 nm laser diode," *Opt. Exp.*, vol. 27, no. 9, pp. 12171–12181, 2019.

[10] C. Fei, X. Hong, G. Zhang, J. Du, Y. Wang, and S. He, "Improving the performance of long reach UOWC with multiband DFT-spread DMT," *IEEE Photon. Technol. Lett.*, vol. 31, no. 16, pp. 1315–1318, Aug. 2019.

[11] F. Wang, Y. Liu, F. Jiang, and N. Chi, "High speed underwater visible light communication system based on LED employing maximum ratio combination with multi-PIN reception," *Opt. Commun.*, vol. 425, pp. 106–112, 2018.

[12] X. Chen, W. C. Lyu, Z. J. Zhang, J. Zhao, and J. Xu, "56-m/3.31-Gbps underwater wireless optical communication employing Nyquist single carrier frequency domain equalization with noise prediction," *Opt. Exp.*, vol. 28, no. 16, pp. 23784–23795, 2020.

[13] T. C. Wu, Y. C. Chi, H. Y. Wang, C. T. Tsai, and G. R. Lin, "Blue laser diode enables underwater communication at 12.4 Gbps," *Sci. Rep.*, vol. 7, 2017, Art. no. 40480.

[14] W. S. Tsai, H. H. Lu, H. W. Wu, C. W. Su, and Y. C. Huang, "A 30 Gb/s PAM4 underwater wireless laser transmission system with optical beam reducer/expander," *Sci. Rep.*, vol. 9, 2019, Art. no. 8605.

[15] C. - Y. Li, H. - H. Lu, Y. - C. Huang, Q. - P. Huang, J. - Y. Xie, and S. - E. Tsai, "50 Gb/s PAM4 underwater wireless optical communication systems across the water–air–water interface [Invited]," *Chin. Opt. Lett.*, vol. 17, no. 10, 2019, Art. no. 100004.

[16] P. Leon et al., "A new underwater optical modem based on highly sensitive silicon photomultipliers," in *Proc. OCEANS Aberdeen*, 2017, pp. 1–6.

[17] L. Zhang et al., "Over 10 attenuation length gigabits per second underwater wireless optical communication using a silicon photomultiplier (SiPM) based receiver," *Opt. Exp.*, vol. 28, no. 17, pp. 24968–24980, 2020.

[18] M. Zhao et al., "Long-reach underwater wireless optical communication with relaxed link alignment enabled by optical combination and arrayed sensitive receivers," *Opt. Exp.*, vol. 28, no. 23, pp. 34450–34460, 2020.

[19] Y. Dai et al., "200-m/500-Mbps underwater wireless optical communication system utilizing sparse nonlinear equalizer with variable step size generalized orthogonal matching pursuit," *Opt. Exp.*, vol. 29, no. 20, pp. 32228–32243, 2021.

[20] C. Fei et al., "100-m/3-Gbps underwater wireless optical transmission using a wideband photomultiplier tube (PMT)," *Opt. Exp.*, vol. 30, no. 2, pp. 2326–2337, 2022.

[21] Z. Wang, D. Tsonev, S. Videv, and H. Haas, "Towards self-powered solar panel receiver for optical wireless communication," in *Proc. IEEE Int. Conf. Commun.*, 2014, pp. 3348–3353.

[22] M. Kong, B. Sun, R. Sarwar, J. Shen, and X. Jing, "Underwater wireless optical communication using a lens-free solar panel receiver," *Opt. Commun.*, vol. 426, pp. 94–98, 2018.

[23] X. Chen et al., "Diversity-reception UWOC system using solar panel array and maximum ratio combining," *Opt. Exp.*, vol. 27, no. 23, pp. 34284–34297, 2019.

[24] J. Fakidis, H. Helmers, and H. Haas, "Simultaneous wireless data and power transfer for a 1-Gb/s GaAs VCSEL and photovoltaic link," *IEEE Photon. Technol. Lett.*, vol. 32, no. 19, pp. 1277–1280, Oct. 2020.

[25] W. H. Shin, S. H. Yang, D. H. Kwon, and S. K. Han, "Self-reverse-biased solar panel optical receiver for simultaneous visible light communication and energy harvesting," *Opt. Exp.,* vol. 24, no. 22, pp. A1300–A1305, 2016.

[26] S. Zhang et al., "Organic solar cells as high-speed data detectors for visible light communication," *Optica*, vol. 2, no. 7, pp. 607–610, 2015.

[27] M. Kong et al., "Toward self-powered and reliable visible light communication using amorphous silicon thin-film solar cells," *Opt. Exp.*, vol. 27, no. 24, pp. 34542–34551, 2019.

[28] M. Kong et al., "AquaE-lite hybrid-solar-cell receiver-modality for energy-autonomous terrestrial and underwater Internet-of-Things," *IEEE Photon. J*, vol. 12, no. 4, Aug. 2020, Art. no. 7904713.

[29] Z. Tong, X. Yang, H. Zhang, Y. Dai, X. Chen, and J. Xu, "Series-connected solar array for high-speed underwater wireless optical links," *Opt. Lett.*, vol. 47, no. 5, pp. 1013–1016, 2022.

[30] Z. Wang, D. Tsonev, S. Videv, and H. Haas, "On the design of a solar-panel receiver for optical wireless communications with simultaneous energy harvesting," *IEEE J. Sel. Areas Commun.*, vol. 33, no. 8, pp. 1612–1623, Aug. 2015.

[31] Z. Kubik and J. Skala, "Stripline for electromagnetic susceptibility testing — Input impedance matching," in *Proc. Int. Conf. Appl. Electron.*, 2017, pp. 1–4.

[32] W. Liu, Y. Yang, L. Meng, Y. Zhu, and Z. Gao, "Limited length coding and improved energy detection for underwater photoelectric signal recovery," *Proc. SPIE*, vol. 58, no. 5, 2019, Art. no. 053104.

[33] J. Saadé, A. Goulahsen, A. Picco, J. Huloux, and F. Pétrot, "Low overhead, DC-balanced and run length limited line coding," in *Proc. IEEE 19th Workshop Signal Power Integrity*, 2015, pp. 1–4.